Role of Nucleolar Factors in Modulating Nuclear Architecture

A thesis

submitted to

Indian Institute of Science Education and Research, Pune

in partial fulfilment of the requirements for the

BS-MS Dual Degree Programme

by

Goury Parvathy J Nair

Indian Institute of Science Education and Research Pune

Dr. Homi Bhabha Road,

Pashan, Pune 411008, INDIA.

April 2020

Supervisor: Kundan Sengupta

Certificate

This is to certify that this dissertation entitled 'Role of Nucleolar Factors in Modulating Nuclear Architecture' towards the partial fulfilment of the BS-MS dual degree programme at the Indian Institute of Science Education and Research, Pune represents work carried out by Goury Parvathy J Nair at Chromosome Biology lab, Indian Institute of Science Education and Research, Pune, under the supervision of Dr. Kundan Sengupta, Department of Biology, during the academic year 2019-2020.
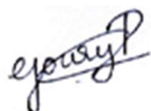
Supervisor

Dr. Kundan Sengupta

Associate Professor

IISER, Pune

Student

Goury Parvathy J Nair

BS-MS student

IISER, Pune

Declaration

I hereby declare that the matter embodied in the report entitled 'Role of Nucleolar Factors in Modulating Nuclear Architecture' are the results of the work carried out by me at the Department of Biology, Indian Institute of Science Education and Research, Pune, under the supervision of Dr. Kundan Sengupta and the same has not been submitted elsewhere for any other degree

Student

Goury Parvathy J Nair

BS-MS student

IISER, Pune

Supervisor

Dr. Kundan Sengupta

Associate Professor

IISER, Pune

Table of Contents

List of Tables and Figures

Abstract

Integral nucleolar proteins such as Nucleolin and Fibrillarin play major roles in regulating nuclear as well as nucleolar structure and function. Nucleolin interacts with other nucleolar components such as Fibrillarin to maintain the distinct phase-separated morphology of the nucleolus. Interestingly, several cancers show a significant upregulation in the levels of Nucleolin. Here, we showed that overexpression of Nucleolin increases the sphericity of the nucleolus while nuclear morphology remains unchanged. However, depletion of another nucleolar protein Fibrillarin showed abnormal nuclear morphology. We also investigated the effect Fibrillarin depletion on nuclear Lamins, as well as its effect on nucleolar morphology and function. Fibrillarin knockdown showed an increase in the transcript levels of Lamin A and Lamin B2. However, Fibrillarin knockdown also showed a collective decrease in the protein levels of all nuclear lamins. We hypothesize that depletion of Fibrillarin also decreases levels of C-MYC, which in turn associates with and potentially downregulates transcript levels of Lamin A and Lamin B2 respectively.

Acknowledgements

Introduction

The mammalian cell nucleus is a membrane-bound organelle containing chromatin and proteins necessary for gene expression. The nucleus contains several sub-nuclear organelles, such as the nucleolus and Cajal bodies (Lamond and Earnshaw, 1998). Nucleolus is the site of ribosomal RNA (rRNA) synthesis, pre-RNA processing and ribosome subunit assembly (Olson et al., 2002). The nucleolus does not have a membrane surrounding it. Nevertheless, the nucleolus maintains its distinct morphology, by the phenomenon of Liquid-liquid phase separation (LLPS). Nucleolar proteins such as nucleolin, fibrillarin, nucleophosmin and nucleostemin, in conjunction with rDNA and RNA, impart a distinct, phase-separated and spherical morphology (Feric et al., 2016; Hyman et al., 2014).

Nucleolin protein is composed of three structural domains that include (i) N-terminal domain with multiple acidic stretches (ii) a central domain with two or more RNA-binding domains (RNA Recognition motifs or RRMs) and (iii) C-terminal GAR (Glycine Arginine Rich) domain.
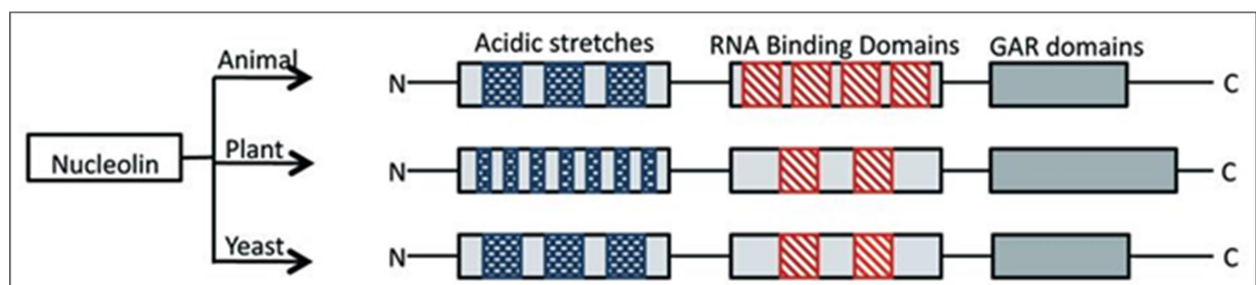
Figure 1: Schematic representation of the primary sequence of nucleolin and nucleolin-like proteins in animal, plant and yeast *(Image adapted from Tajrishi 2011).*

Nucleolin is one of the most abundant non-ribosomal proteins in the cell (Andersen et al., 2005). Nucleolin is involved in diverse functions ranging from rDNA transcription and ribosomal assembly as shown in mammalian cultured cells (Bouvet et al., 1998; Cong et al., 2012). Depletion of nucleolin affects nucleolar morphology (Ma et al., 2007). Another nucleolar protein, nucleophosmin (NPM1), modulates liquid-liquid phase separation of the nucleolus via heterotypic interactions with

ribosomal RNA as well as other nucleolar proteins with Arginine-rich motifs, such as SURF6 (Mitrea et al., 2018).

Fibrillarin is another key nucleolar protein essential for pre-RNA processing that methylates RNAs and proteins (Tessarz et al., 2014; Tollervey et al., 1991). It consists of a Glycine-Arginine Rich (GAR domain) at its N-terminal, a central domain with sequence similarity to RNA Recognition Motifs (RRMs) and C-terminal alpha-helical domain.
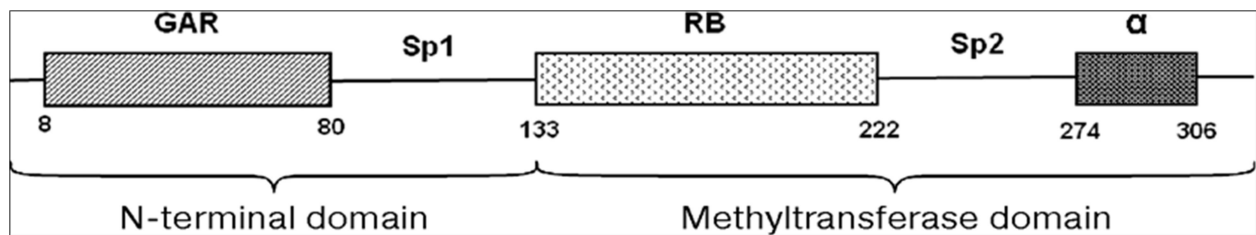
Figure 2: Schematic representation of the primary sequence of Fibrillarin. *(Image adapted from Shubina 2016)*

Several nuclear envelope proteins also affect the nucleolus and vice versa. Depletion of SUN1 shows nucleolar hypertrophy and decreased rRNA synthesis (Matsumoto et al., 2016). Lamin B1 depletion also resulted in decrease in rRNA synthesis and induced structural changes within the nucleolus (Martin et al., 2009). While Lamin B2 knockdown results in nucleolar aggregates, overexpression of nucleolin rescues disrupted nucleolar morphology (Sen Gupta and Sengupta, 2017). Fibrillarin is also necessary for a spherical nuclear morphology and cell proliferation (Amin et al., 2007). Interestingly, fibrillarin knockdown affects the morphology of the nucleus as it shows an increase in the frequency of nuclear invaginations.

The nucleolus is organized around ribosomal DNA (rDNA) that encodes for ribosomal RNA (rRNA). The primary RNA coded by the rDNA is 45S, which is further processed to give rise to 18S, 28S and 5.8S rRNAs. These constitute the RNA component of ribosomes (Moore and Steitz, 2002). rDNA transcription is confined to the nucleolus, and the processed rRNA products constitute a major structural and catalytic part of the ribosome (Moore and Steitz, 2002; Russell and Zomerdijk, 2005). rRNA accumulation is mainly regulated at the level of rDNA transcription by RNA Polymerase I (Grummt, 2003). Since the rate of cell growth is linked to the rate of

protein synthesis, which is in turn linked to the rate of ribosome biogenesis, regulation of rDNA transcription plays a determining role in the growth and proliferation of cells (Moss, 2004; Ruggero and Pandolfi, 2003).

Several nucleolar components regulate rRNA transcription. Many nucleolar proteins such as Nucleolin and Fibrillarin are involved in rRNA biosynthesis (Chen and Huang 2001). Nucleophosmin acts as a nucleolar histone chaperone and regulates transcription of rDNA (Murano et al., 2008).

Here we examine the impact of Nucleolin - a protein enriched at the granular component at the border of the nucleolus - on nucleolar morphology, while we also investigate into the role of another nucleolar protein - Fibrillarin (localized in the dense fibrillar component) on nuclear morphology.

Materials and Methods

Cell Culture

Frozen DLD1 colorectal adenocarcinoma cells were thawed in a 37°C water bath for 2 minutes. Thawed cells are transferred to fresh RPMI media and centrifuged at 1000 rpm for 5 min to discard DMSO - a cryoprotectant. Cells were incubated overnight at 37°C, with 5% CO_2. The cell culture media was first discarded followed by DPBS (1 ml) washes. 1 ml of 0.05% Trypsin was added to the plate and incubated at 37°C for 5 min until the cells detach. Fresh RPMI (~2 ml) was added to neutralize the trypsin. The cells were centrifuged at 1000 rpm for 5 minutes. The cells were cultured at 37°C in a T25 flask.

Cell Seeding

Cells diluted 1:10 (10 μl + 90 μl media), were counted in a hemocytometer.

DNA Transfection

250 μl Opti-MEM, 2 μg plasmid DNA and 2 μl PLUS Reagent was added in a 1.5 ml vial (A). To another vial (B), 250 μl Opti-MEM and 5 μl LTX reagent was added. Both tubes were vortexed and incubated at RT for 5 minutes. The contents of A was added to B, vortexed again, centrifuged followed by incubation for 30 minutes at RT and added to cells along with 1.5 ml media. Cells were incubated at 37°C, with 5% CO_2 for 24 hours.

RNA Transfection

All siRNAs were used at a concentration of 100 nM. 250 μl Opti-MEM and 20 μl of 10 μM siRNA was taken in a 1.5 ml eppendorf tube (A). In another 1.5 ml eppendorf tube (B), 250 μl Opti-MEM and 5 μl Lipofectamine RNAiMAX was taken. Both tubes were vortexed and incubated at RT for 5 minutes. The contents of A was added to B, vortexed again and given a short spin. The transfection mix was then incubated for 30 minutes at RT. The mix was then added to the well along with 1.5ml media. Cells were incubated at 37°C, with 5% CO_2 for 24 hours. The media was changed after 24 hours of knockdown. Cells were further processed 48 hours after transfection.

MG132 Treatment

Cells were subjected to siRNA mediated knockdown for 48 hours followed by MG132 treatment (5 µM) for 24 hours (5 µl of MG132 (stock concentration of 20 mM) was diluted in 1.5 µl DMSO). This was added to each well containing 2 ml media. 2 µl DMSO was used as the control.

Immunofluorescence Assay

Media was discarded and cells were washed twice with 1X PBS (pH 7.4), for 5 minutes each. Cells were fixed in 4% PFA (pH = 7.2) and incubated for 10 minutes at RT, followed by 2 washes of 1X PBS for 5 minutes each. Cells were blocked in 1 ml 1%BSA (prepared in 1X PBS pH 7.2), for 30 minutes at RT. Cells were washed twice with 1 ml 1X PBS (pH 7.2), for 5 minutes each. Primary antibody diluted in 0.1% BSA, (~40-50 µl) was applied to a parafilm, onto which cells on coverslip was inverted, and incubated in a humidified chamber and incubated for 90 minutes at RT. Cells were washed thrice with 1ml 1X PBS, for 5 minutes each, followed by secondary antibody diluted in 1X PBS for 1 hour at RT. Cells were washed thrice with 1ml 1X PBS, for 5 minutes each and incubated in 1 ml DAPI (0.05 µg/ml) for 2 minutes at RT, followed by two washes in 1 ml 1X PBS, for 5 minutes each and mounted on a clean glass slide with antifade.

Microscopy

Fixed cells were imaged on Zeiss LSM710 confocal microscope or Zeiss Multiphoton microscope with 405nm, 488nm, and 561nm laser lines using a 63X Plan-Apochromat oil immersion objective (NA 1.4), digital zoom of 2.5, pixel depth of 8 and the scan speed was set at 9 and line averaging at 4.

Whole Cell Lysate

Modified RIPA was prepared as follows: 1µl of 50X Protease Inhibitor Cocktail in 50 µl Radio Immunoprecipitation Assay buffer.

1X RIPA buffer reagents	Volume	Final Concentration
NaCl (1 M)	1.5 ml	150 mM

Nonidet P-40	0.1 ml	1%
Sodium deoxycholate	0.05 ml	0.5%
SDS	0.01 ml	0.1%
Tris (50mM, pH 7.4)	5 ml	25 mM
H$_2$O	Make up to 10 ml	-

Media was discarded and cells were washed with 1ml PBS. 50 µl of modified RIPA lysis buffer was added. Using a cell scraper, cells were thoroughly scraped off. This lysate was placed on ice for 5 mins and centrifuged at 4°C, 14,000 rpm for 15 minutes. The supernatant was collected into fresh vials and stored at -80°C.

Protein Assay Using Bicinchoninic Acid

BCA Protein Assay Kit (#23225), reagents A and B and were diluted in a concentration of 50:1 (A:B). 10µl standard and 200µl BCA mix were added. 5µl Modified RIPA buffer, 5µl 1X PBS and 200µl BCA mix were added as blank. For test samples, 5µl lysate was added to 5µl 1x PBS and 200µl BCA mix. All samples were in duplicates. The plate was incubated at 37°C for 30 minutes. Readings were taken on a spectrophotometer at 562nm.

Western Blot

A 10% gel was prepared and samples were prepared from protein lysates, in accordance with BCA estimation calculations. Samples were heated at 95°C for 10 minutes and loaded, along with ladder. The tank was filled with 1L of Running Buffer. The gel was resolved at 80 V, and at a higher voltage of 120V in the resolving phase.

Reagents (For SDS-PAGE gel)	Resolving (10%)	Stacking (5%)
Distilled Water	2.95 ml	2.1 ml
Acrylamide/Bisacrylamide (30%)	2.5 ml	495 µl
Tris (1.5M)	1.9 ml (pH 8.8)	375 µl (pH 6.8)

SDS (20%)	37.5 µl (0.1%)	15 µl (0.1%)
APS (10%)	75 µl (0.1%)	30 µl (0.1%)
TEMED	5 µl	3 µl

Transfer SDS-PAGE Gel was placed in contact with the methanol-activated PVDF membrane and was transferred for 1.5 hours at 70-80 V. **Blocking** Membrane was blocked with 5% skimmed milk, prepared in TBST, for 1 hour (or overnight). After blocking, three washes with 1X TBST, for 10 minutes each. **Primary Antibody** The membrane was incubated in primary antibody diluted in 0.5% skimmed milk. Blots were sealed in plastic pouches with diluted primary antibody and incubated at 4°C overnight. Blots were washed thrice in 1X TBST for 10 minutes each. **Secondary Antibody** HRP-tagged antibody was diluted in a 1:10,000 ratio with 0.5% milk and incubated at RT for 1 hour Followed by three washes in 1X TBST for 10 minutes each. **Detection** (Amersham™ ECL™ Prime) Western Blotting Detection Reagent kit (RPN2232), Solution A (luminol) and Solution B (Peroxide) were added in a 1:1 ratio. 1 ml of this solution was pipetted upon the blot and developed by chemiluminescence.

RNA Isolation

Adherent cells were washed with ice-cold 1X PBS. 1 ml TRIzol was added to each well of a 6-well plate and pipetted 5-6 times. The contents were then transferred to a 1.5 ml vial and vortexed for 15 seconds. The vial was incubated at RT for 5 minutes. 200 µl chloroform was added to the vial and vortexed for 15 seconds, followed by incubation at RT for 5 minutes, centrifuged at 12,000 g for 15 minutes, at 4°C. To the aqueous layer equal volume of isopropanol was added and mixed by inverting several times, followed by incubation at RT for 15 minutes and then spun down at 12,000g for 15 minutes at 4°C. Isopropanol was discarded and 1 ml of 75% ethanol was added to the pellet and resuspended, centrifuged at 12,000 g for 15 minutes, at 4°C. Pellet was air-dried and resuspended in 10-15 µl nuclease free water. RNA was quantified using NanoDrop at 260nm.

cDNA Synthesis

cDNA synthesis was performed using Thermo Scientific™ Verso cDNA Synthesis Kit

RT mix (A)	Volume (µl)	Final Concentration (after A+B)
5x cDNA synthesis buffer	4	1X
dNTP mix (5 mM)	2	500 µM
Verso RT enhancer (500 ng/µl)	1	25 ng/µl
Verso enzyme mix	1	
NFW	7	-
Total	15	-

RNA Mix (B)	For 1 µg
Oligo dT	1 µl
RNA	1 µg (Upto 4 µl)
NFW	Make up to 5 µl
Total	5 µl

The RNA mix was incubated at 70°C for 5 min and quickly chilled in ice for 5 min. 15µl RT mix (A) was added to the RNA mix. The following program was set up for the PCR scheme for the synthesis of cDNA.

Annealing	25°C	15 min
Extension	42°C	60 min
RT enzyme inactivation	70°C	5 min
Hold	4°C	-

qRT-PCR

The prepared cDNA was diluted at 1:1 with NFW. qRT-PCR was set up with KAPA SYBR Green with 5 µl reaction mix per well.

Reagent	Stock Concentration	Volume	Final Concentration
NFW	-	1.3 µl	-
Primer (F+R)	5 µM	0.2 µl	0.2 µM
KAPA SYBR	2X	2.5 µl	1X
cDNA	-	1.0 µl	-
Total	-	5.0 µl	-

The RT-PCR plate was sealed with a micro-sealer and was spun at 800 rpm for 2 minutes. The plate was then loaded onto BIORAD Real-time PCR detection system. The instrument was rum according to the following program:

| Step		Temperature	Time
A	Hot start reaction	95°C	3 min
B	Denaturation	95°C	20 sec
C	Annealing and Data Acquisition	60°C	1 min
D	Repeat Cycle (B and C)	35 X	
E	Determination of melt curve from 60 to 95	0.5°C/cycle	
F	Hold	4°C	∞

Statistical analysis and graphs

Graphs were plotted and statistical analyses were done using GraphPad Prism 5 software. Measure of significance was calculated using Mann-Whitney (non-parametric) test. A minimum of 30 cells were analysed, for each biological replicate. All experiments were performed in a minimum of N=2 independent biological

replicates. Number of technical replicates (n) differs for each experiment and is indicated.

Image Processing and Analysis

Quantifications of fluorescence intensities were performed using Fiji ImageJ. All fluorescence intensity quantification other than line scans were by selecting the area of the nucleus in the mid-optical section using the DAPI channel and finding the mean fluorescence intensity in the respective channel to be quantified.
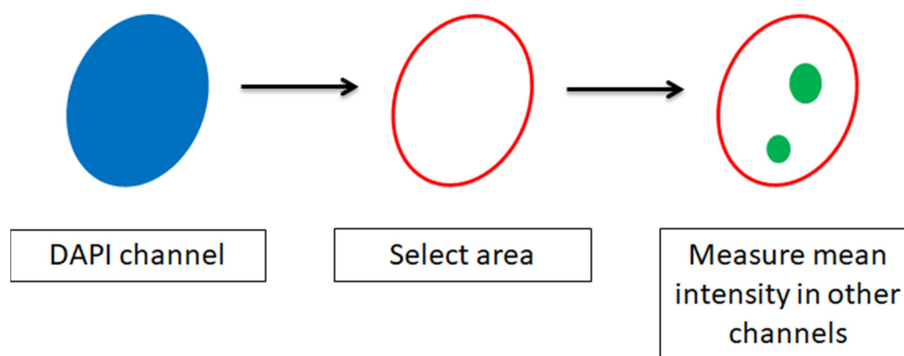
Line scans were performed by drawing a line through the midpoint of the nucleus in the mid-optical section
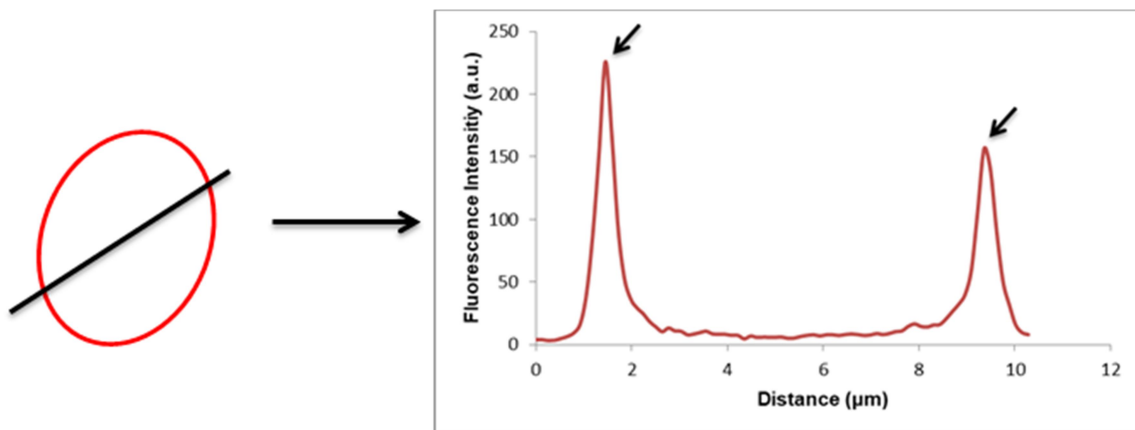
Nuclear and nucleolar topological measurements were quantified using Huygens Image Analyser. Images were reconstructed in 3D and object Analyser tool was used to quantify topological parameters such as (i) volume (ii) sphericity and (iii) surface area

Plasmid DNA

Addgene pE-GFP-N1 (5169 bp) and NCL-GFP (6453 bp) were used as control and for Nucleolin overexpression, respectively.

Cell lines and cell culture

DLD-1 cells were kind gifts from the laboratory of Dr.Thomas Ried (NCI/NIH, Bethesda, USA). Human colorectal adenocarcinoma cells DLD-1 were grown in RPMI1640 (Gibco 11875) supplemented with heat inactivated 10% FBS (Gibco 6140) and Penicillin (100 units/ml)/Streptomycin (100 µg/ml) (Gibco, 15070-063). Cells were maintained in 5% CO_2 at 37 °C.

Primary antibody

Antibody	Catalogue No.	Dilution	Application
Anti-Mouse Lamin B2	ab50887	1:500	Western blot, IFA
Anti-Mouse Fibrillarin	ab1416	1:1000	Western blot
Anti-Rabbit Fibrillarin	ab92547	1:1000	IFA
Anti-Mouse Nucleolin	ab54893	1:1000, 1:500	Western blot, IFA
Anti-Rabbit Lamin B1	ab16048	1:1000, 1:500	Western blot, IFA
Anti-Rabbit GAPDH	Sigma G9545	1:10,000	Western blot
Anti-Rabbit LMNB1	ab16048	1:1000	IFA

Secondary antibody

| Antibody	Catalogue No.	Dilution	Application
Goat anti mouse-Alexa 488	Invitrogen A11029	1:1000	IFA
Goat anti mouse-Alexa 568	Invitrogen A11004	1:1000	IFA
Goat anti Rabbit-Alexa 568	Invitrogen A11011	1:1000	IFA
Goat anti Rabbit-Alexa 488	Invitrogen A11034	1:1000	IFA
Donkey Anti- Rabbit IgG HRP	GE Amersham NA9340V	1: 10000	Western blot
Sheep Anti- Mouse IgG HRP	GE Amersham NA9310V	1:10000	Western blot

Results

Role of nucleolin in regulating nucleolar morphology

It is well established that nucleoli within the nucleus exist as independent, phase-separated and spherical entities (Hult et al., 2017). Most normal cells have at least 2-3 independent nucleoli. However, cancer cells typically have multiple nucleoli, 5 or more, which correlates with an increased cell proliferation (Farley et al., 2015). Nucleolar morphology and numbers are characteristic features that serve as diagnostic parameters for cancers (Derenzini et al., 1998, Derenzini et al., 2009). Nucleolar proteins such as nucleolin and its association with DNA/RNA, among others, are involved in liquid-liquid phase separation and therefore the morphology of the nucleolus (Mitrea et al., 2018, Feric et al., 2016). Here we examined the role of nucleolin - a granular component protein - in regulating the morphology of the nucleolus.

To study the factors that regulate nucleolar morphology, we examined the effect of overexpressing GFP-tagged nucleolin in otherwise diploid colorectal cancer cells - DLD1. Cells transfected with the empty vector - pE-GFP-N1 served as control. We performed immunoblotting which showed a distinctive endogenous band corresponding to that of nucleolin migrating at ~110 kDa, while the fluorescently tagged GFP-nucleolin migrated at a relatively higher molecular weight of ~150 kDa (Fig 3). Imaging of cells was performed to examine the extent of nucleolin overexpression in DLD1 cells (Fig 3 A,B). Immunofluorescence assay was performed inorder to examine nuclear and nucleolar morphology respectively at the level of single cells (Fig 3C). We imaged DLD1 cells overexpressing nucleolin-GFP and compared the same with that of control cells (vector alone). We also counted the number of nucleoli in each nucleus, which remains unchanged in both the nucleolin overexpressing and control DLD1 cells (Fig 3D). Confocal imaging of single nuclei and nucleoli, followed by 3D reconstructions (Fig 3E) and measurements, revealed a significant increase in nucleolar sphericity (Fig 3G) (Nucleolar sphericity, vector control = 0.70 and NCL-OE = 0.74, p-value = 0.0005). Interestingly, independent measurements showed that Nucleolin overexpression does not affect nucleolar

volume (Fig 3F). We similarly measured nuclear volume and sphericity, which did not show a change upon NCL-GFP overexpression in DLD1 cells (Fig 3H,I). Taken together, this suggests that an increase in nucleolin levels alters nucleolar morphology by decreasing nucleolar volume and rendering a more compact and spherical morphology to the nucleolus, while the nucleolar numbers or the nuclear morphology remains largely unaffected.
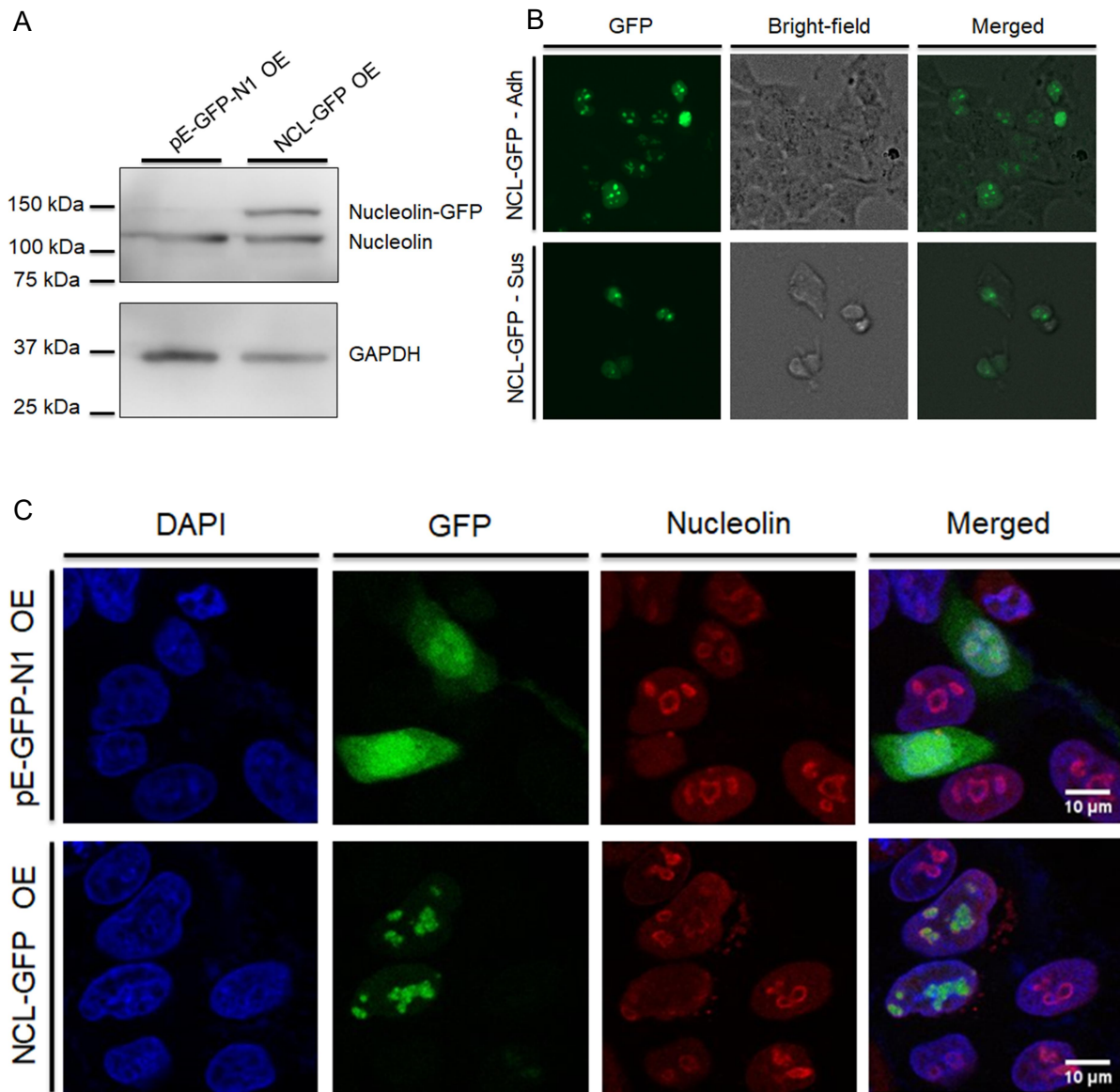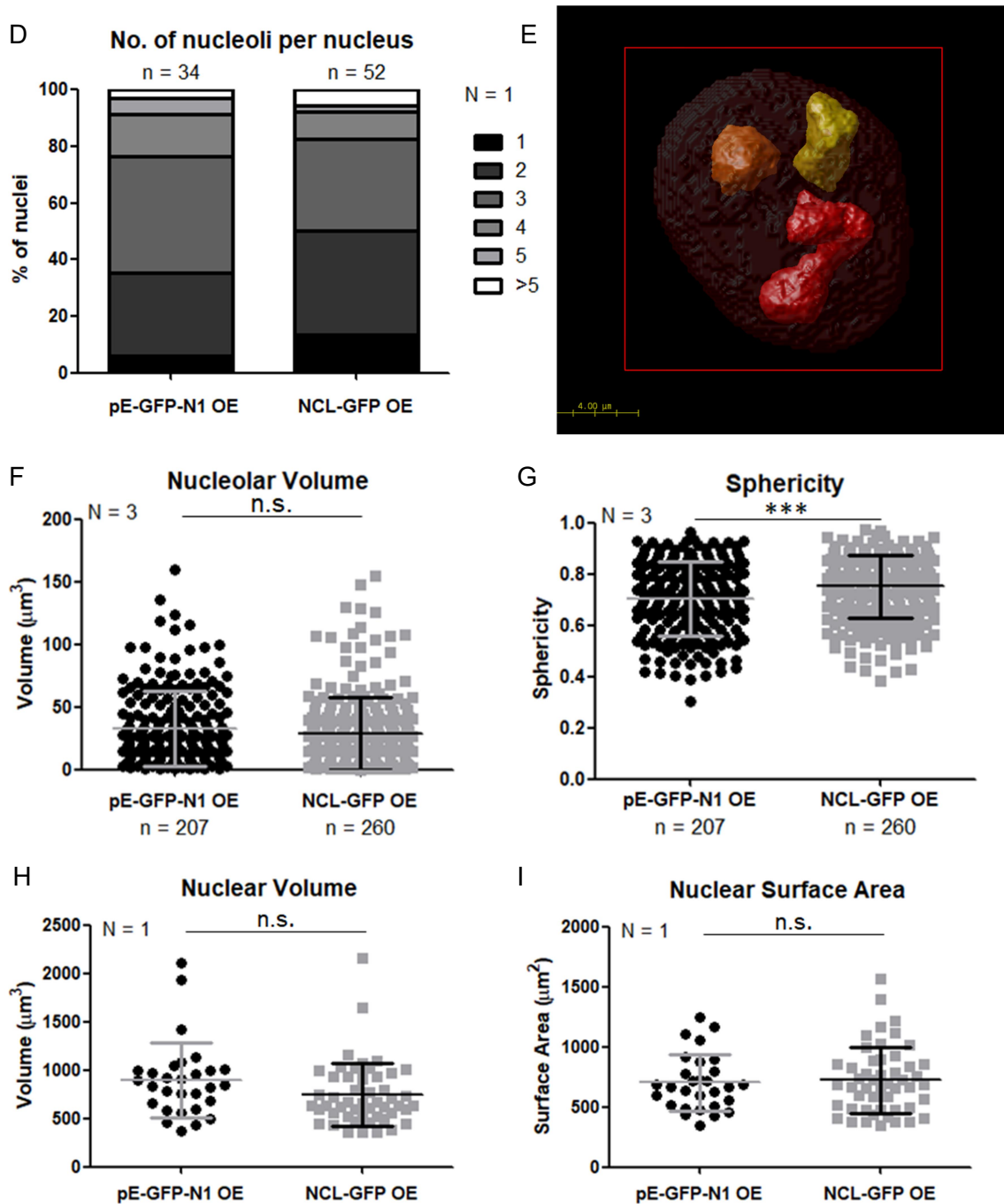
Fig 3 : Overexpression of GFP-tagged Nucleolin (A) Confirmation of NCL-GFP Overexpression in DLD-1 cells with western blot. The higher molecular weight band in the second lane corresponds to NCL-GFP. (B) Live-cell images of cells transfected with pE-GFP-N1 or NCL-GFP. Efficiency of transfection is ~51.3% for pE-GFP-N1 and ~35.5% for NCL-GFP. (C) Immunofluorescence images of cells transfected with pE-GFP-N1 or NCL-GFP. Blue channel corresponds to DAPI, green channel GFP and red channel Nucleolin. (D) Number of nucleoli per nucleus in NCL-

GFP overexpressed cells does not show a significant change. (E) Representative image of 3D reconstructions using Z-stacks. (F) Nucleolar volume does not change upon NCL-GFP OE. (G) Nucleolar sphericity increases upon NCL-GFP OE. (H) Nuclear volume does not change significantly upon NCL-GFP OE. (I) Comparison of nuclear surface area in control and NCL-GFP OE cells. Nuclear surface area does not change significantly upon NCL-GFP OE.

Effect of Fibrillarin and Lamin knockdowns on transcript levels of lamins and nucleolar targets

As discussed in the preceding section, we found a specific effect of overexpressing nucleolin, which showed a distinctive change in nucleolar morphology but not on nuclear morphology. We next examined the effect of perturbing the levels of another bonafide nucleolar protein - Fibrillarin, to study if this affects nuclear morphology and nucleolar function. Fibrillarin-depleted cells show abnormal non-spherical nuclear morphology (Amin et al., 2007). Work from the Chromosome Biology Lab (CBL) has revealed that fibrillarin loss induces aberrant nuclear morphology in terms of nuclear invaginations (Sen Gupta A, unpublished results).

We therefore investigated the underlying mechanisms of fibrillarin induced changes at the nuclear lamina. We also asked if there exists a possible feedback mechanism at the transcript level between FBL and Lamins. We therefore performed qRT-PCR to determine if FBL Kd affects transcript levels of Lamin genes and vice-versa. Knockdown of nuclear lamins (Lamin A, Lamin B1, Lamin B2) and Fibrillarin was performed independently in DLD1 cells using siRNA to determine the transcript level changes on nuclear, as well as nucleolar genes targets (Fig 4).

A Lamin A levels

B Lamin B1 levels

C Lamin B2 levels

D LBR levels

E FBL levels
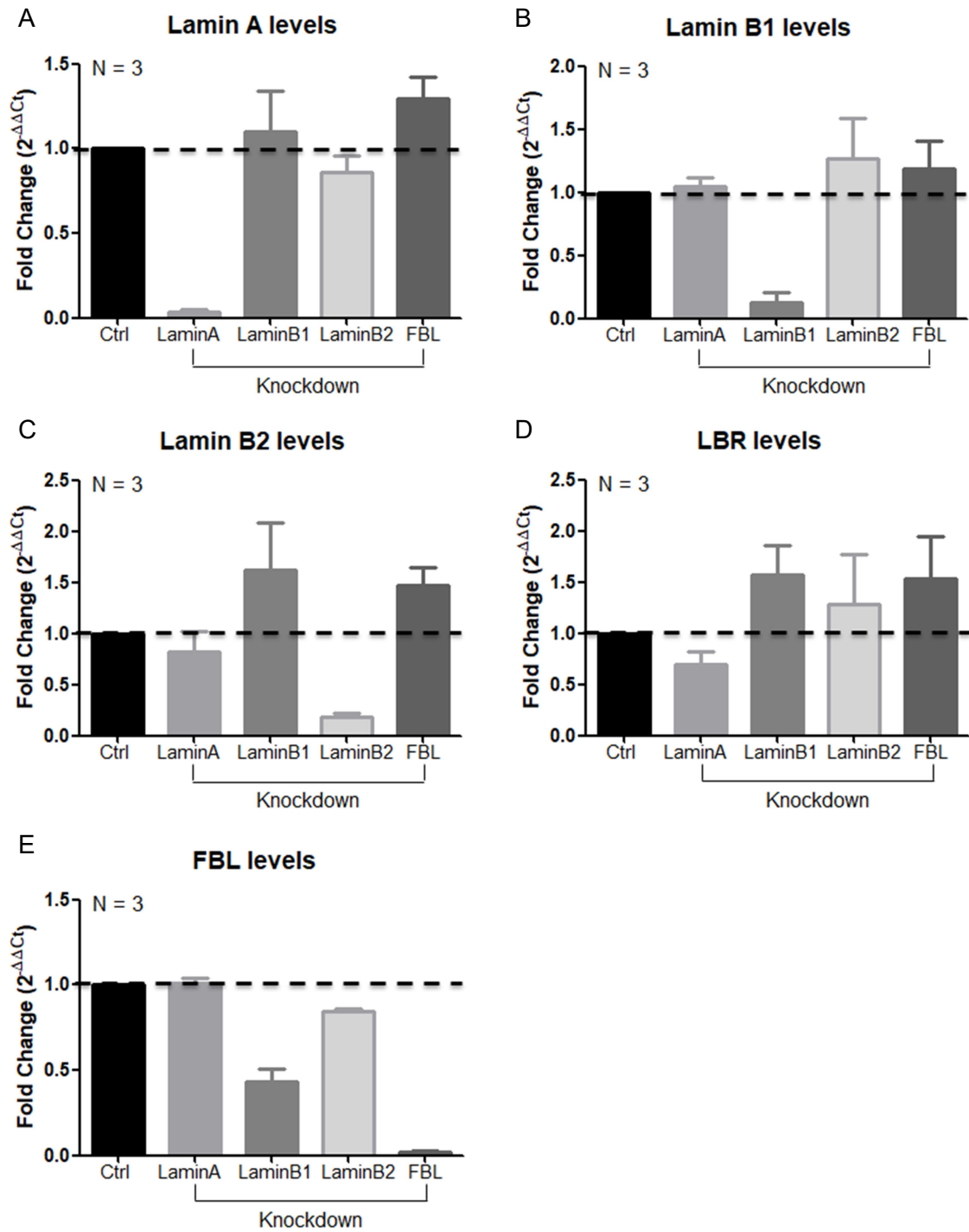
Knockdown	Lamin A	Lamin B1	Lamin B2	FBL	LBR
Lamin A	>95% ↓	-	-	-	~30% ↓
Lamin B1	-	~87% ↓	-	~57% ↓	~29% ↑
Lamin B2	~14% ↓	-	~82% ↓	~15% ↓	-

| FBL | ~30% ↑ | - | ~48% ↑ | >95% ↓ | ~53% ↑ |

Fig 4: qRT-PCR showing transcript level changes in LMNA, LMNB1, LMNB2, LBR and FBL *(A-E) RT-PCR graphs show changes in the levels of each transcript. (F) Table depicting deregulation in the levels of each transcript for each knockdown.*

Analysis of C-MYC binding regions

As mentioned previously FBL depletion deregulates transcript levels of both Lamin A and Lamin B2, but not Lamin B1 (Fig 5). To understand more about the mechanism responsible for this effect, we examined the status of transcription factors that regulate lamin expression levels upon FBL Kd. Previous in-silico analyses in the lab identified MYC as a transcription factor downregulated upon FBL depletion. We, therefore, examined publically available ChIP-seq data (WashU EpiGenome Browser) to determine if c-Myc shows an occupancy upstream of TSS of the lamin and LBR genes.

Interestingly, c-Myc was enriched upstream of the TSS of both *LMNA* and *LMNB2* genes (Fig 5A,C). *LMNA* gene shows c-Myc enrichment ~420 bp upstream of TSS, whereas *LMNB2* shows C-Myc enrichment ~155 bp upstream of TSS. Interestingly, c-Myc was enriched upstream of the TSS of *LMNB1* (Fig 5B). *LBR* gene did not show a specific enrichment of c-Myc close to its TSS (Fig 5D). In summary, these analyses suggest that Fibrillarin depletion might alter the occupancy of C-MYC and therefore the expression levels of Lamin A and Lamin B2.
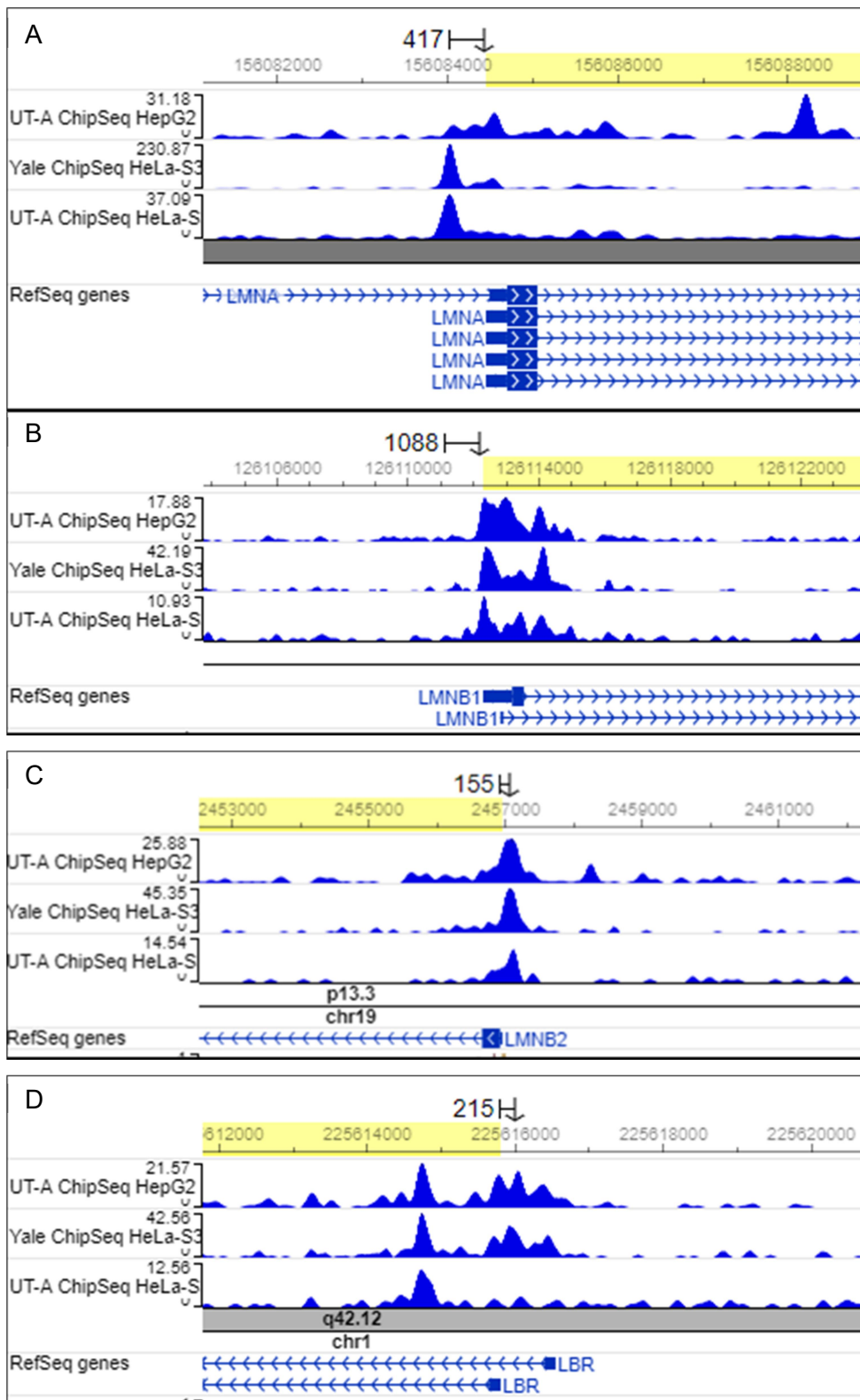
Fig 5: ChIP-seq data from WashU EpiGenome Browser showing c-Myc enrichment close to the TSS of Lamins and LBR Blue peaks indicate the enrichment of c-Myc close to the TSS of (A) LMNA, (B) LMNB1, (C) LMNB2 and (D)

Effect of Fibrillarin and Lamin knockdowns on transcript levels of ribosomal DNA

As discussed in the previous sections (Fig 4), Fibrillarin depletion affects lamin levels. We next examined the effect of FBL depletion on nucleolar function, by monitoring levels of rRNA. Changes in the rate of rDNA transcription directly affect the rate of ribosome synthesis, which leads to changes in rate of protein synthesis (Grummt, 2003). This, in turn, affects cell proliferation (Moss, 2004; Ruggero and Pandolfi, 2003). Thus, quantifying rRNA transcript levels gives an insight into the functional significance of fibrillarin.

We performed qRT-PCR to determine if depletion of FBL and Lamins affected the levels of the rRNA. Knockdown of nuclear lamins (Lamin A, Lamin B1, Lamin B2) and Fibrillarin was performed independently in DLD-1 cells using siRNA to study the transcript level changes on rDNA genes with siLacZ as the control. qRT-PCR was used to estimate the changes in the level of transcripts with B2M as a control (Fig 6)

While FBL Kd did not affect rDNA transcription, knockdown of both Lamin B1 and Lamin B2 increased the levels of 45s rRNA significantly (Fig 6C). Depletion of Lamin A also has an effect on 18s rRNA levels, but not on 28s or 45s rRNAs (Fig 6A). Taken together, this indicates that while the bonafide nucleolar gene FBL does not affect the expression of rDNA genes, interestingly enough nuclear lamins affect transcriptional regulation of rDNA genes (Fig 6).

A 18s rRNA Transcript levels

B 28s rRNA Transcript levels

C 45s rRNA Transcript levels
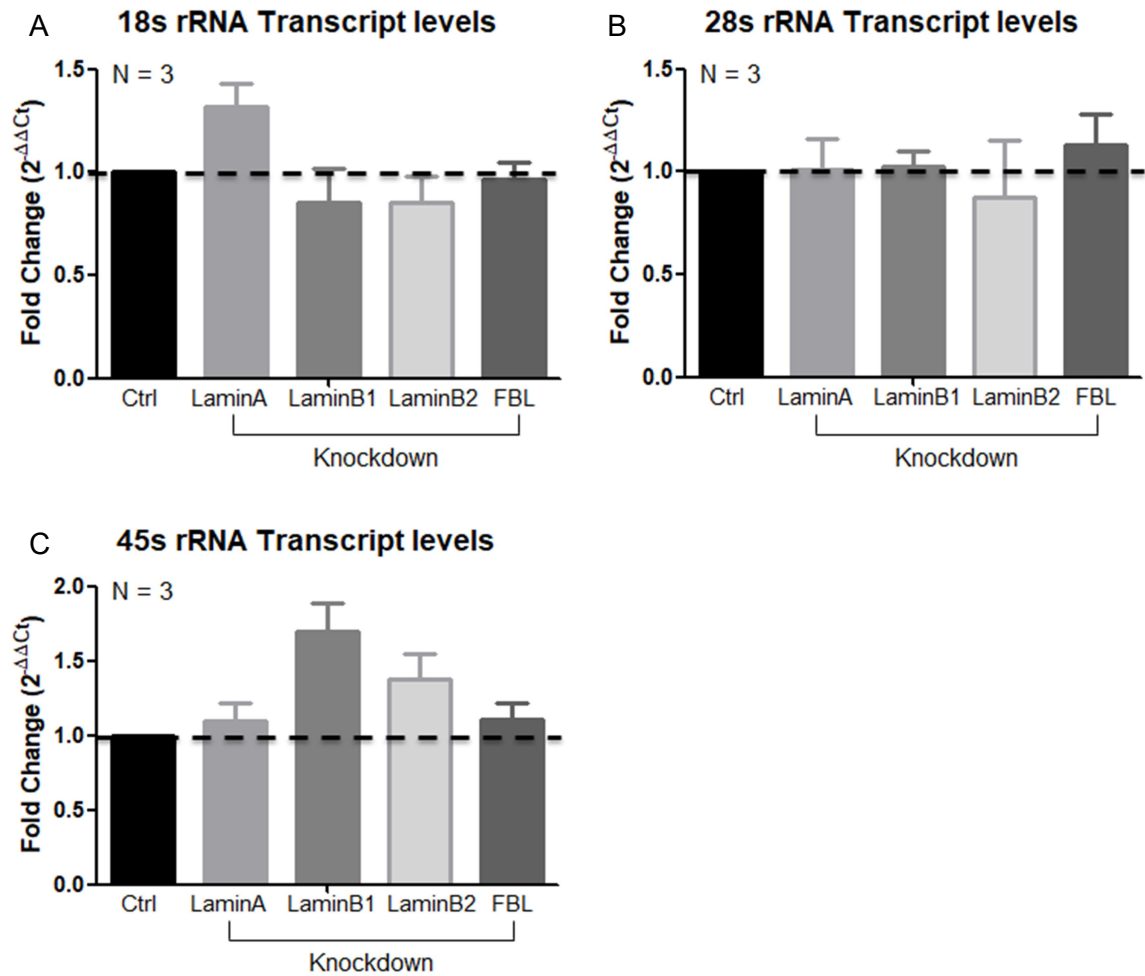
Knockdown	18s rRNA	28s rRNA	45s rRNA
Lamin A	~ 32% ↑	-	-
Lamin B1	-	-	~ 69% ↑
Lamin B2	-	-	~ 38% ↑
FBL	-	-	-

Fig 6: qRT-PCR showing transcript level changes in 18s rRNA, 28srRNA and 45s rRNA *(A-C) RT-PCR graphs show changes in the levels of each transcript. (D) Table depicting deregulation in the levels of each transcript for each knockdown.*

Effect of MG132 treatment on transcript levels of Lamins and FBL upon Lamin, FBL knockdowns

As mentioned in the previous section, we found that lamin depletion impacts fibrillarin expression and vice versa (Fig 4). We next asked if a proteasomal inhibitor such as MG132, also impacts gene expression levels. MG132 (carbobenzoxy-Leu-Leu-leucinal) is a peptide aldehyde that blocks the proteolytic activity of the 26S proteasome complex (Guo and Peng 2013). Treatment of cells with MG132 alters the localization of nucleolar factors such as Nucleophosmin (Latonen et al. 2011).

Interestingly, MG132 treatment shows a significant decrease in Lamin A/C and B1 upon all knockdowns other than control (Fig 7A,B). MG132 showed a decrease in Lamin A/C levels upon FBL Kd (~10%) (Fig 7A). MG132 treatment also decreased transcript levels of Lamin B2 upon Lamin A and FBL knockdown (Fig 7C). However the fold changes of these downregulations are small (~5% decrease).
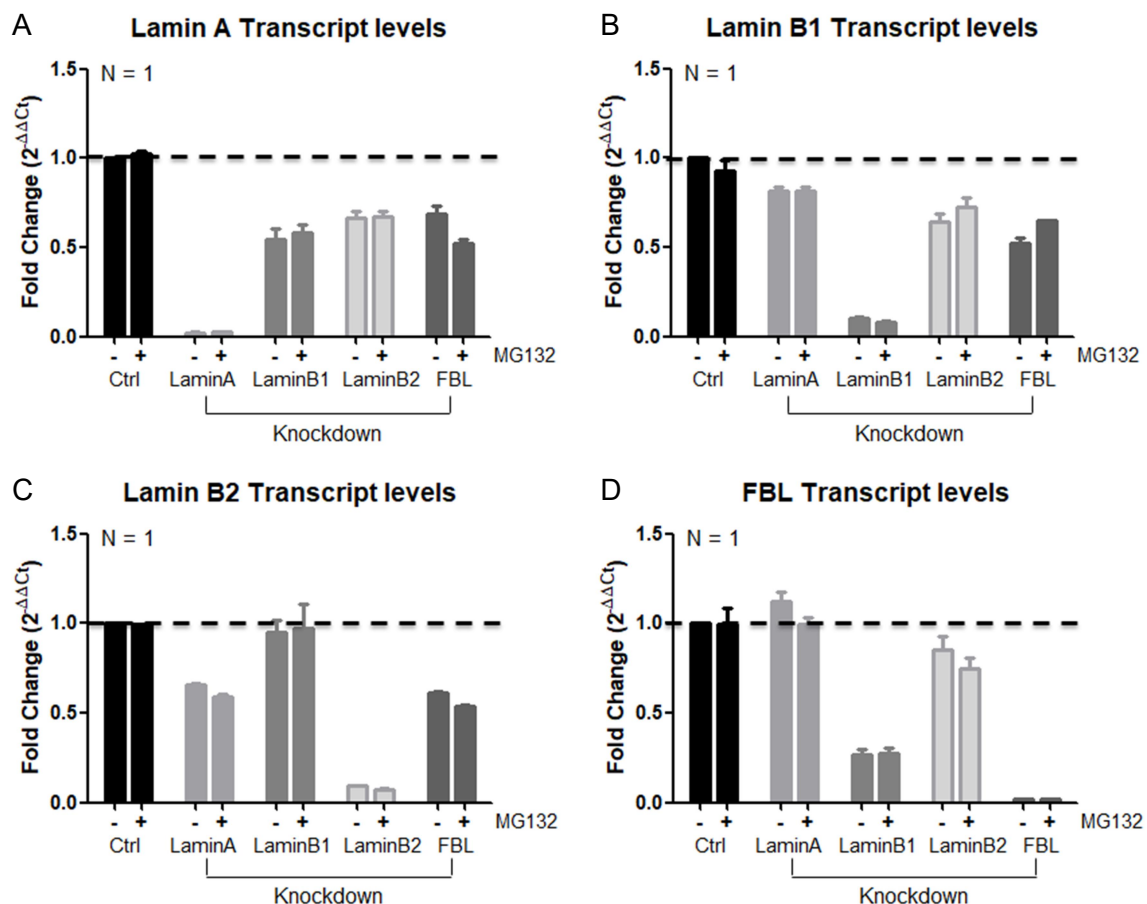
Fig 7: qRT-PCR showing transcript level changes in Lamin A, Lamin B1, Lamin B2 and FBL upon Lamin and FBL knockdowns and MG132 treatment *(A-D) RT-PCR graphs show changes in the levels of each transcript.*

Effect of MG132 treatment on transcript levels of ribosomal DNA upon Fibrillarin and Lamin knockdowns

Next, we examined the effect of MG132 treatment on rRNA levels upon lamin and FBL knockdowns. MG132 inhibits pre-RNA processing and therefore depletes the levels of 18s and 28s rRNA (Stavreva et al. 2006). We examined the effect of MG132-inhibition of ubiquitin proteasomal activity in the background of lamin depletion on rRNA transcript levels.

As noted earlier (Fig 6), knockdown of both Lamin B1 and Lamin B2 significantly increased the levels of 45s rRNA. Interestingly, MG132 treatment significantly decreased the levels of 45s rRNA transcripts in both Lamin B1 and Lamin B2 knockdowns (Fig 8A). MG132 treatment also decreased the level of 18s rRNA, which had increased significantly upon Lamin A Kd (Fig 8C). However, levels of 28s rRNA showed a huge amount of variation across the two replicates (Fig 8B). MG132 treatment showed upregulation of 28s transcript levels in both Lamin A and FBL Knockdowns and downregulation in Lamin B1 and Lamin B2 knockdowns.
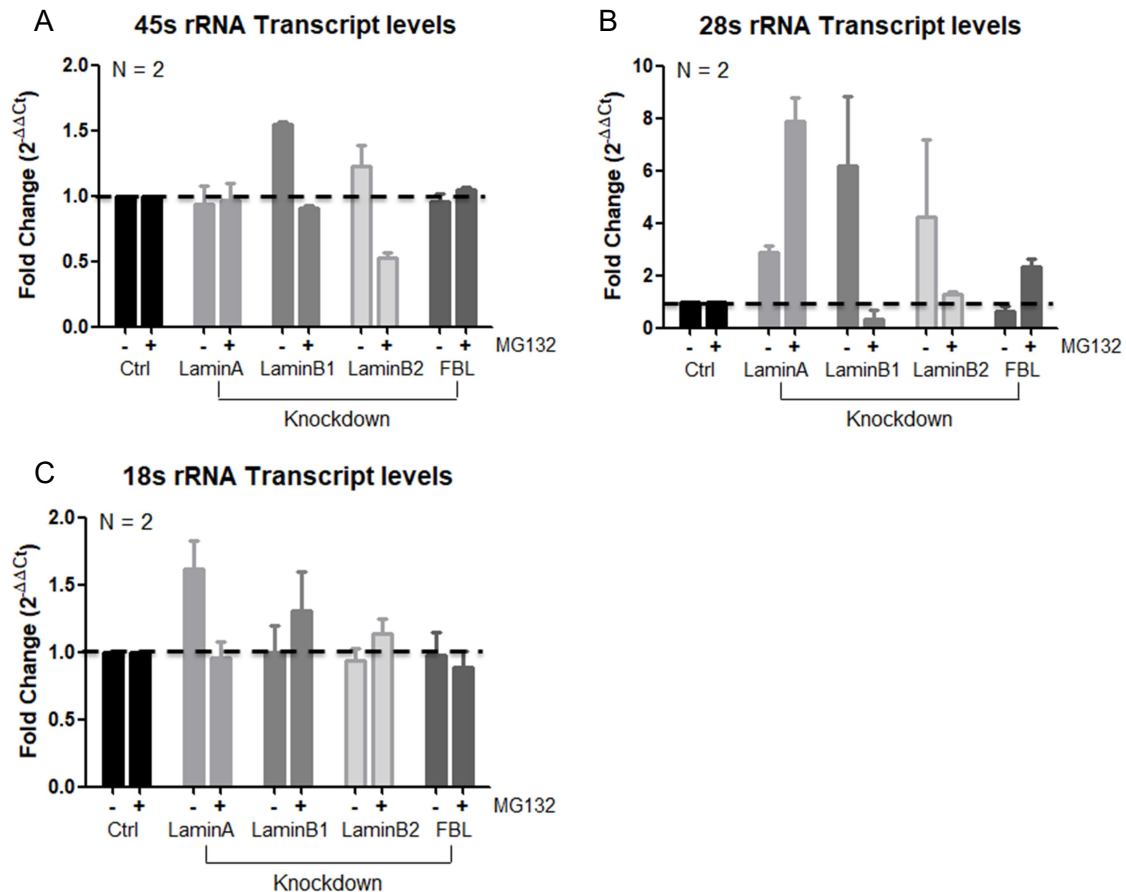
Fig 8: qRT-PCR showing transcript level changes in 18s rRNA, 28srRNA and 45s rRNA upon Lamin and FBL knockdowns and MG132 treatment *(A-C) RT-PCR graphs show changes in the levels of each transcript.*
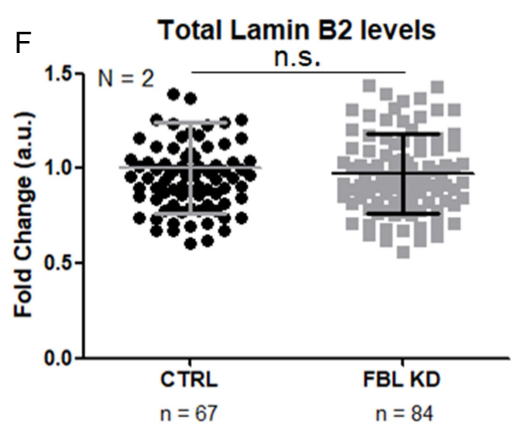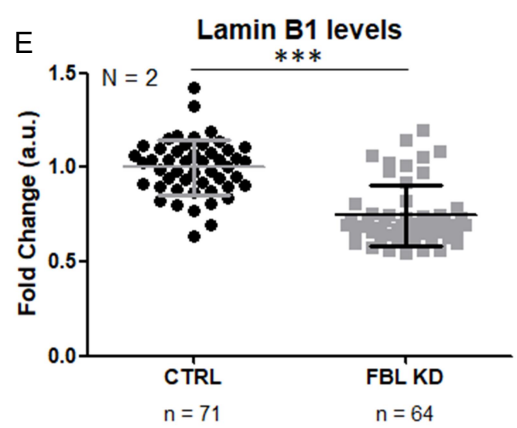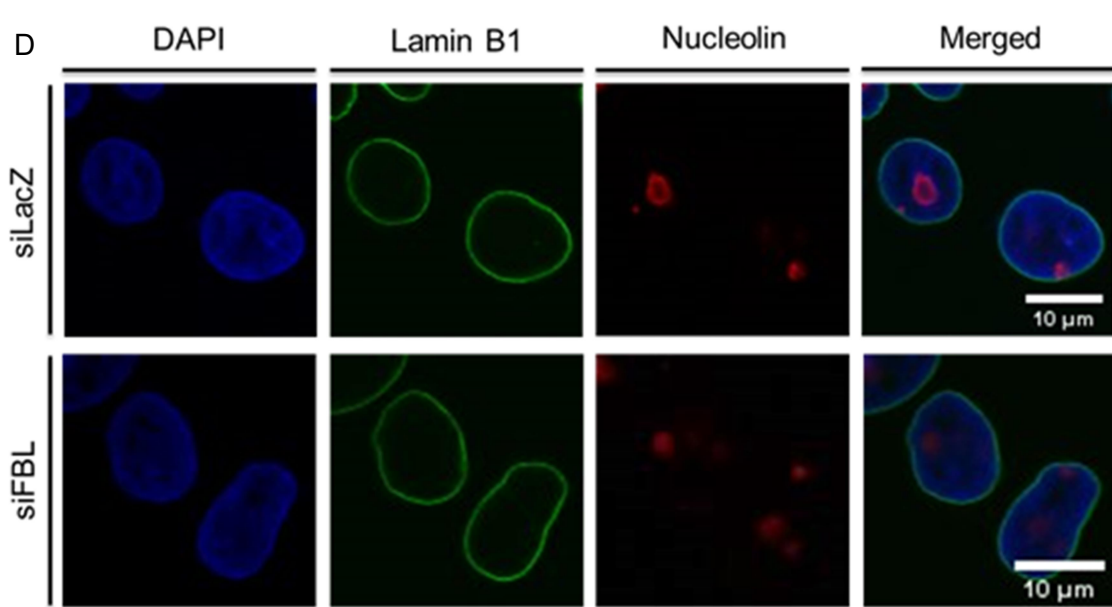
Effect of Fibrillarin knockdown on Lamin levels and localization

We found the effect of Fibrillarin depletion on lamin transcript levels, specifically, that there is an increase in the transcript levels of Lamin A and Lamin B2 upon FBL Kd (Fig 4). We performed Fibrillarin knockdown in DLD1 cells using siRNA to study if Fibrillarin loss impacts the morphology of the nucleus. To achieve this, we examined the effect of FBL Kd on the levels of lamins - one of the major proteins of the nuclear envelope, that imparts mechanical strength and integrity to the nucleus (Dechat et al., 2010). A non-targeting siLacZ oligonucleotide served as control. Western blot was used to determine the knockdown efficiency of Fibrillarin and to determine protein levels of fibrillarin and nuclear lamins upon FBL Kd (Fig 8A,B). Knockdown efficiency of Fibrillarin was ~75% (Fig 8B). FBL Kd decreased the protein levels of all

lamins significantly. Lamin A and Lamin C decreased by ~30% upon FBL Kd, whereas Lamin B1 decreased by ~ 27%. Levels of Lamin B2 also decreased by ~30% upon FBL Kd. Immunofluorescence assay was also performed after FBL Kd to examine the levels of Lamin B1 and Lamin B2, along with nucleolar proteins namely - FBL and Nucleolin (Fig 8C,D). Levels of Lamin B1 decreased significantly upon FBL Kd (Fig 8E). (Fold change ~0.27, P-value<0.0001). Levels of Lamin B2 did not change upon FBL KD (Fig 8F). However, analyses of Lamin B2 at the single cell level shows a significant decrease in Lamin B2 levels at the nuclear periphery upon FBL Kd (Fig 8G) (Fold change ~0.30, P-value<0.0001). Nucleolin protein level did not change significantly upon FBL Kd (Fig 8H). Taken together, these results suggest that levels of Lamins decrease upon FBL depletion at the protein level.

Taken together, the results show the effect of perturbation of key nucleolar proteins on nuclear and nucleolar architecture. Overexpression of Nucleolin increased the sphericity of the nucleoli but did not affect nuclear morphology. Depletion of Fibrillarin showed an increase in the transcript levels of Lamin A/C and Lamin B2, whereas depletion of either Lamin B1 or Lamin B2, decreased in transcript levels of Fibrillarin. In summary, these results suggest the existence of a transcriptional feedback mechanism between the B-type lamins and Fibrillarin (FBL), implying a crosstalk between the nuclear envelope and the nucleolus
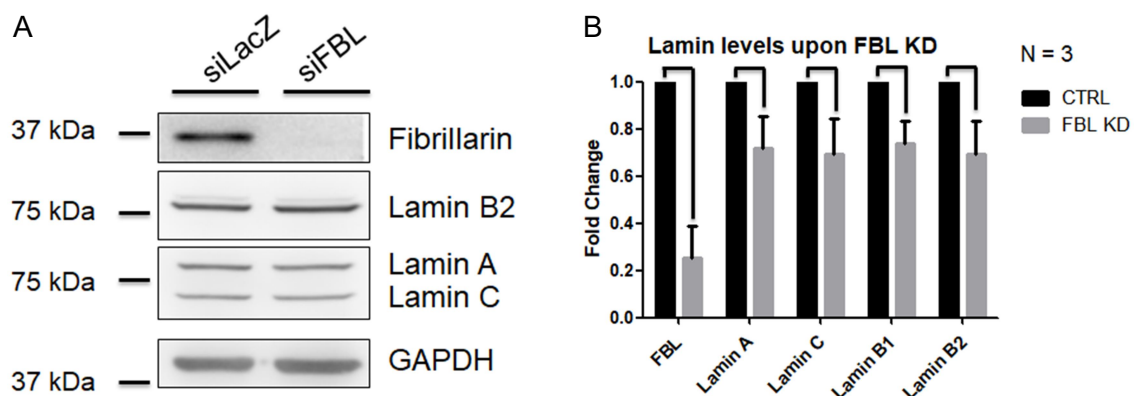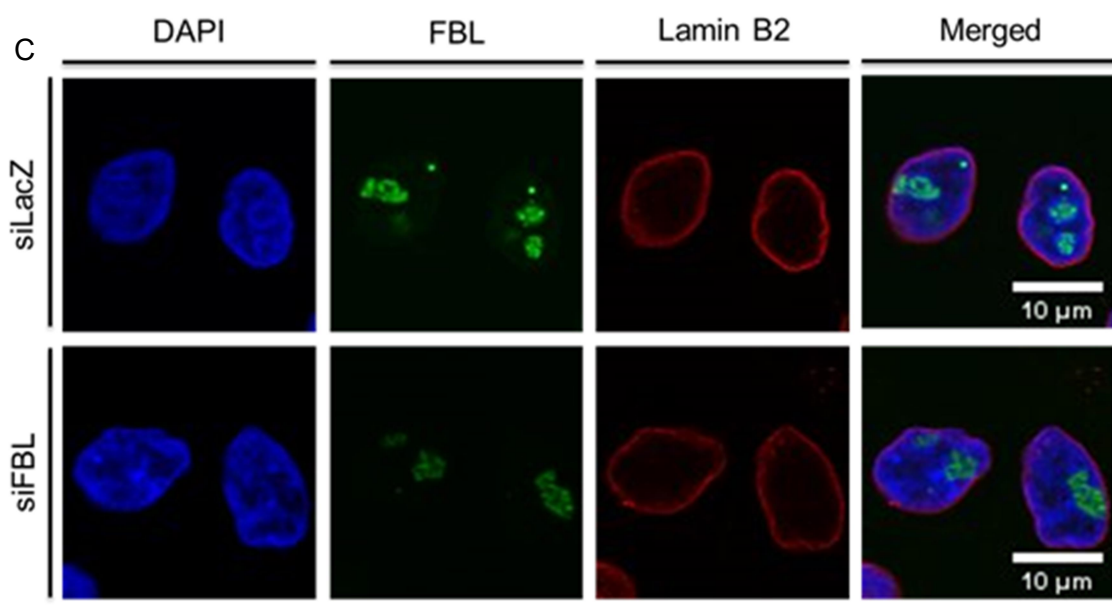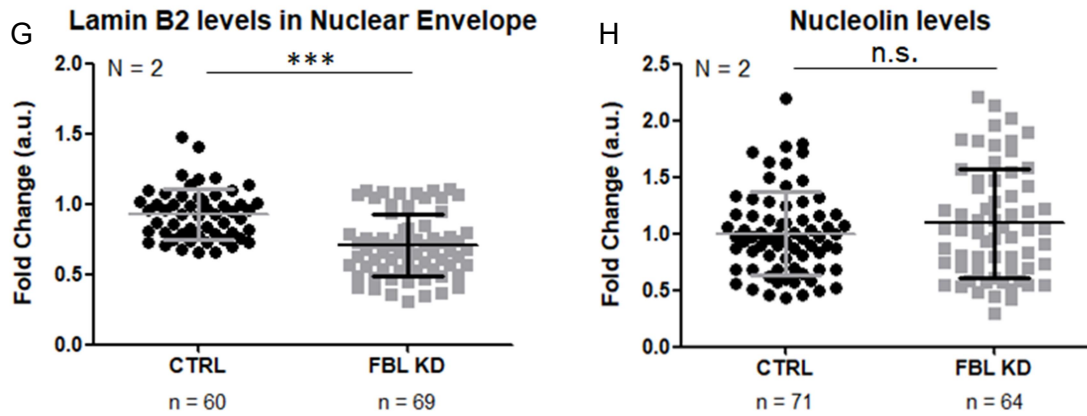
Fig 9: Effect of Fibrillarin knockdown on protein levels of Lamins and Nucleolin *(A) Western blot showing FBL knockdown. (B) Quantification of band intensities in (A), the knockdown efficiency of Fibrillarin was ~75%. (C) Immunofluorescence assay for Lamin B2 and FBL upon FBL KD. DAPI (blue), FBL (green) and Lamin B2 (red) (D) Immunofluorescence assay for Lamin B1 and NCL upon FBL Kd. DAPI (blue), Lamin B1 (green) and NCL (red) (E) Lamin B1 levels in control and FBL Kd cells. Fold change is ~0.27. P<0.0001. (F) Lamin B2 levels in control and FBL Kd cells. Does not change significantly. (G) Lamin B2 at the nuclear envelope. Fold change ~0.3. P<0.0001. (H) Nucleolin levels in control and FBL Kd cells. No significant change in levels of Nucleolin levels.*

Discussion

Several studies suggest that the size and number of nucleoli show an increase in cancer cells. Nucleolar numbers vary from an average of ~2 per nucleus (HCT116) to 6 nucleoli (T98G) or 8 nucleoli per nucleus (U2OS) in cancer cells (Farley et al., 2015). Increase in nucleolar area per nucleus directly correlates with RNA Polymerase I activity (Derenzini et al., 1998). While changes in nucleolar area and number have been reported from several cell lines, the exact reason for these wide variations in nucleolar morphology and function are unclear.

Malignant cells have irregularly shaped nucleoli (Pianese et al. 1896). Nucleolar size is a prognostic indicator to differentiate between malignant and benign tumors in a number of cancers as nucleolar size is thought to reflect the rate of cell proliferation (Derenzini et al., 1998, 2009).

Deregulated expression of Nucleolin has also been observed in different cancer cell types. Upregulation of Nucleolin has been observed in a variety of tumor tissues, including colorectal cancer (Hammoudi et al., 2013), gastric cancer (Qiu et al., 2013) and breast cancer (Berger et al., 2015). Whether this increase is a cause or consequence of tumor progression is unclear. Increased number and size of nucleoli is frequently seen in several malignant tumors. This is most likely reflective of the increased rate of ribosome biogenesis in these tumors. These changes might also reflect on the total amount of the major nucleolar proteins, such as Nucleolin, in these tumors.
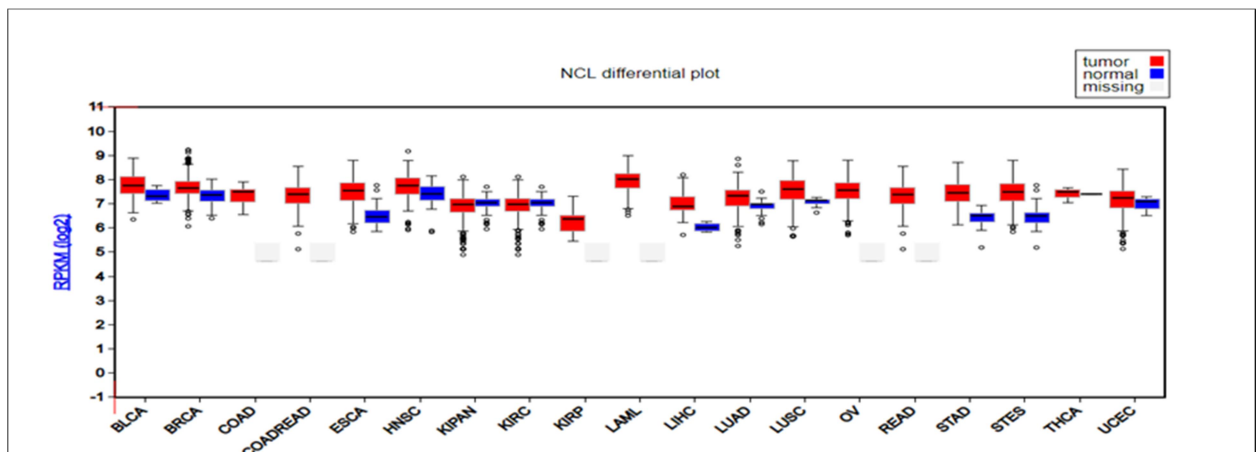
Fig 10: Expression profile of Nucleolin in cells from different parts of the body
Red indicates tumor and blue indicates normal cells.

Nucleolin overexpression showed an increase in nucleolar sphericity (Fig 3). However, it does not seem to affect nucleolar numbers or volume. This increase in nucleolar sphericity could point towards an increase in the compactness of nucleoli upon NCL OE. There is evidence suggesting that liquid-liquid phase separation plays an important role in the formation and maintenance of the distinct, spherical morphology of the nucleolus (Feric et al., 2016). Nucleophosmin interacts with other nucleolar proteins such as NCL, GNL3 and SURF6 via two acidic tracts in its Intrinsically disordered regions (IDRs) to maintain the phase-separated morphology of the nucleolus (Mitrea et al., 2016, 2018). This interaction could be strengthened with the increased amount of nucleolin in the Nucleolin overexpressed system. This might lead to the nucleoli being further compacted. Lamin B2 depletion increases nucleolin aggregation in the nucleoplasm (Sen Gupta and Sengupta, 2017).

Perturbing Nucleolin levels in the cell has no effect on nuclear morphology. However, Fibrillarin knockdown is known to cause changes in nuclear morphology (Amin et al., 2007). FBL knockdown increases the transcript levels of Lamin A and Lamin B2, but not Lamin B1. Transcriptional regulation of the genes *LMNA* and *LMNB2* by a transcription factor is a possible mechanism by which the above changes are effected. Previous work by Ayantika Sen Gupta, PhD student from Chromosome Biology Lab, had identified *MYC* as a transcription factor, which is deregulated upon FBL knockdown (Fig 9). Interestingly, the consensus binding site of *MYC* (identified as CACGTG) is near the transcription start site (2 kb upstream to 1 kb downstream of the TSS) of all lamins (Fig 10). Using ChIP-Atlas, we also identified that *MYC* was enriched specifically 2 kb upstream or 1 kb downstream of Lamin A and Lamin B2, whereas this enrichment was not found in Lamin B1 (Fig 8). Taken together, this suggests that FBL is involved in regulating transcript levels of specific lamins, namely, Lamin A/C and Lamin B2, but not Lamin B1.
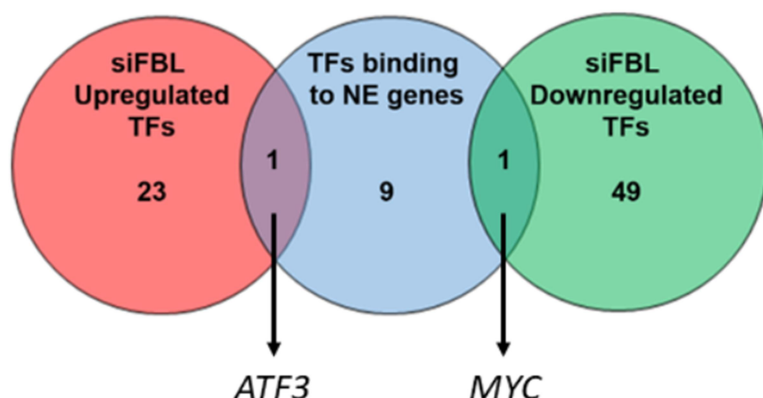
Fig 11: Overlap of transcription factors (T.F.s) affected upon Fibrillarin knockdown, with T.F.s regulating nuclear architectural genes affected by Fibrillarin knockdown *(Adapted from Sen Gupta, Ayantika, 2018 (Doctoral Thesis) 'Role of nuclear Lamins in the regulation of nucleolar structure and function' Chromosome Biology Lab, IISER, Pune)*
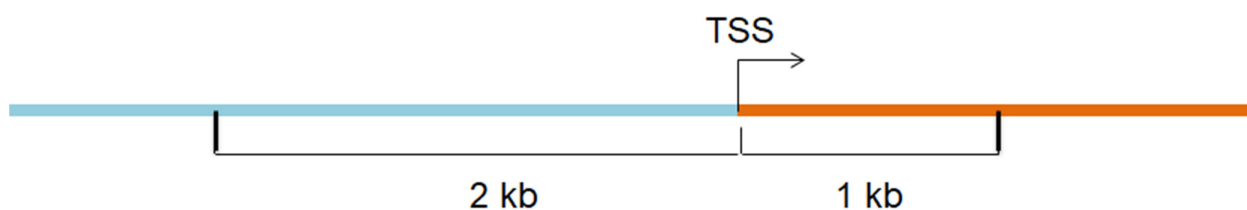

Fig 12: Pictorial representation of region classified as 'near' to TSS of a gene to identify enrichment of a transcription factor

Myc regulates rDNA transcription and nucleolar morphology. c-Myc and another transcription factor Max interact in the nucleoli to recruit RNA polymerase I and initiate rDNA transcription (Arabi et al., 2005; Grandori et al., 2005). c-Myc also interacts with Nucleophosmin and this interaction is essential for proper localization of c-Myc in the nucleolus (Li and Hann, 2013).

Interestingly, while FBL depletion shows an increase in transcript levels of Lamin B2 and not Lamin B1, knockdowns of both B-type Lamins show a downregulation in the transcript levels of FBL. Lamin B1 knockdown, specifically, shows an approximately 50% reduction in the level of FBL transcripts. It is interesting to note that depletion of Lamin B1 results in fibrillarin aggregates to form in the nucleoplasm (Martin et al.,

2009). Lamin B2 depletion shows a smaller effect on FBL transcript levels (~15% reduction). Lamin A depletion also shows no effect on FBL transcript levels.

While FBL is involved in ribosome biosynthesis (Rodriguez-Corona et al., 2015), FBL depletion seemingly has no effect on rRNA transcript levels. However, Lamin depletion seems to have an effect on transcriptional regulation of rDNA genes. B-type Lamins, specifically, upregulate levels of 45s rRNA, whereas levels of 18s and 28s rRNAs remain unchanged. This effect of Lamin B2 depletion on 45s rRNA levels has been shown before (Sen Gupta and Sengupta, 2017). This result strengthens the notion that lamins play a major role in regulating nucleolar architecture as well as function.

MG132 is a potent proteasome inhibitor that binds to 20S proteasome and effectively inhibits the proteolytic activity of the 26S proteasome (Guo and Peng 2013). MG132 inhibits tumor cell proliferation by inducing cell cycle arrest and triggering apoptosis (Chen and Huang 2001). MG132 shows a decrease in the levels of Lamin B2 upon Lamin A and FBL knockdowns. Furthermore, MG132 decreased the levels of Lamin A in FBL depleted cells. MG132 treatment shows a collective decrease in 45S rRNA (upon B1, B2 depletion) and 18S rRNA upon Lamin A knockdown respectively..

However, FBL depletion decreases the protein levels of all lamins. It is likely that different, independent mechanisms govern the transcript and protein levels of lamins. At a single-cell level, FBL depletion shows a decrease in the levels of Lamin B1. While total levels of Lamin B2 does not change in the nucleus, Lamin B2 levels at the nuclear envelope decreased upon FBL knockdown. This suggests a possible relocalization of Lamin B2 within the nucleus, as a small sub-population of Lamin B2 at the nuclear envelope might be relocalizing to the nucleoplasm.

Taken together, these studies have provided novel insights into the role of nucleolin in regulating nucleolar but not nuclear morphology, while fibrillarin has a marked impact not only on nuclear morphology but also on nucleolar function.

References

Amin, M.A., Matsunaga, S., Ma, N., Takata, H., Yokoyama, M., Uchiyama, S., and Fukui, K. (2007). Fibrillarin, a nucleolar protein, is required for normal nuclear morphology and cellular growth in HeLa cells. Biochem. Biophys. Res. Commun. *360*, 320–326.

Andersen, J.S., Lam, Y.W., Leung, A.K.L., Ong, S.-E., Lyon, C.E., Lamond, A.I., and Mann, M. (2005). Nucleolar proteome dynamics. Nature *433*, 77–83.

Arabi, A., Wu, S., Ridderstråle, K., Bierhoff, H., Shiue, C., Fatyol, K., Fahlén, S., Hydbring, P., Söderberg, O., Grummt, I., et al. (2005). c-Myc associates with ribosomal DNA and activates RNA polymerase I transcription. Nat. Cell Biol. *7*, 303–310.

Berger, C.M., Gaume, X., and Bouvet, P. (2015). The roles of nucleolin subcellular localization in cancer. Biochimie *113*, 78–85.

Bouvet, P., Diaz, J.J., Kindbeiter, K., Madjar, J.J., and Amalric, F. (1998). Nucleolin interacts with several ribosomal proteins through its RGG domain. J. Biol. Chem. *273*, 19025–19029.

Cong, R., Das, S., Ugrinova, I., Kumar, S., Mongelard, F., Wong, J., and Bouvet, P. (2012). Interaction of nucleolin with ribosomal RNA genes and its role in RNA polymerase I transcription. Nucleic Acids Res. *40*, 9441–9454.

Dechat, T., Adam, S.A., Taimen, P., Shimi, T., and Goldman, R.D. (2010). Nuclear lamins. Cold Spring Harb. Perspect. Biol. *2*, a000547.

Derenzini, M., Trerè, D., Pession, A., Montanaro, L., Sirri, V., and Ochs, R.L. (1998). Nucleolar function and size in cancer cells. Am. J. Pathol. *152*, 1291–1297.

Derenzini, M., Montanaro, L., and Treré, D. (2009). What the nucleolus says to a tumour pathologist. Histopathology *54*, 753–762.

Farley, K.I., Surovtseva, Y., Merkel, J., and Baserga, S.J. (2015). Determinants of mammalian nucleolar architecture. Chromosoma *124*, 323–331.

Feric, M., Vaidya, N., Harmon, T.S., Mitrea, D.M., Zhu, L., Richardson, T.M., Kriwacki, R.W., Pappu, R.V., and Brangwynne, C.P. (2016). Coexisting liquid phases underlie nucleolar subcompartments. Cell *165*, 1686–1697.

Grandori, C., Gomez-Roman, N., Felton-Edkins, Z.A., Ngouenet, C., Galloway, D.A., Eisenman, R.N., and White, R.J. (2005). c-Myc binds to human ribosomal DNA and stimulates transcription of rRNA genes by RNA polymerase I. Nat. Cell Biol. *7*, 311–318.

Grummt, I. (2003). Life on a planet of its own: regulation of RNA polymerase I transcription in the nucleolus. Genes Dev. *17*, 1691–1702.

Hammoudi, A., Song, F., Reed, K.R., Jenkins, R.E., Meniel, V.S., Watson, A.J.M., Pritchard, D.M., Clarke, A.R., and Jenkins, J.R. (2013). Proteomic profiling of a mouse model of acute intestinal Apc deletion leads to identification of potential novel biomarkers of human colorectal cancer (CRC). Biochem. Biophys. Res. Commun. *440*, 364–370.

Hult, C., Adalsteinsson, D., Vasquez, P.A., Lawrimore, J., Bennett, M., York, A., Cook, D., Yeh, E., Forest, M.G., and Bloom, K. (2017). Enrichment of dynamic chromosomal crosslinks drive phase separation of the nucleolus. Nucleic Acids Res. *45*, 11159–11173.

Hyman, A.A., Weber, C.A., and Jülicher, F. (2014). Liquid-liquid phase separation in biology. Annu. Rev. Cell Dev. Biol. *30*, 39–58.

Lamond, A.I., and Earnshaw, W.C. (1998). Structure and function in the nucleus. Science *280*, 547–553.

Li, Z., and Hann, S.R. (2013). Nucleophosmin is essential for c-Myc nucleolar localization and c-Myc-mediated rDNA transcription. Oncogene *32*, 1988–1994.

Martin, C., Chen, S., Maya-Mendoza, A., Lovric, J., Sims, P.F.G., and Jackson, D.A. (2009). Lamin B1 maintains the functional plasticity of nucleoli. J. Cell Sci. *122*, 1551–1562.

Matsumoto, A., Sakamoto, C., Matsumori, H., Katahira, J., Yasuda, Y., Yoshidome, K., Tsujimoto, M., Goldberg, I.G., Matsuura, N., Nakao, M., et al. (2016). Loss of the integral nuclear envelope protein SUN1 induces alteration of nucleoli. Nucleus *7*, 68–83.

Ma, N., Matsunaga, S., Takata, H., Ono-Maniwa, R., Uchiyama, S., and Fukui, K. (2007). Nucleolin functions in nucleolus formation and chromosome congression. J. Cell Sci. *120*, 2091–2105.

Mitrea, D.M., Cika, J.A., Guy, C.S., Ban, D., Banerjee, P.R., Stanley, C.B., Nourse, A., Deniz, A.A., and Kriwacki, R.W. (2016). Nucleophosmin integrates within the nucleolus via multi-modal interactions with proteins displaying R-rich linear motifs and rRNA. Elife *5*.

Mitrea, D.M., Cika, J.A., Stanley, C.B., Nourse, A., Onuchic, P.L., Banerjee, P.R., Phillips, A.H., Park, C.-G., Deniz, A.A., and Kriwacki, R.W. (2018). Self-interaction of NPM1 modulates multiple mechanisms of liquid-liquid phase separation. Nat. Commun. *9*, 842.

Moore, P.B., and Steitz, T.A. (2002). The involvement of RNA in ribosome function. Nature *418*, 229–235.

Moss, T. (2004). At the crossroads of growth control; making ribosomal RNA. Curr. Opin. Genet. Dev. *14*, 210–217.

Murano, K., Okuwaki, M., Hisaoka, M., and Nagata, K. (2008). Transcription regulation of the rRNA gene by a multifunctional nucleolar protein, B23/nucleophosmin, through its histone chaperone activity. Mol. Cell. Biol. *28*, 3114–3126.

Olson, M.O.J., Hingorani, K., and Szebeni, A. (2002). Conventional and nonconventional roles of the nucleolus. Int. Rev. Cytol. *219*, 199–266.

Qiu, W., Zhou, F., Zhang, Q., Sun, X., Shi, X., Liang, Y., Wang, X., and Yue, L. (2013). Overexpression of nucleolin and different expression sites both related to the prognosis of gastric cancer. APMIS *121*, 919–925.

Rodriguez-Corona, U., Sobol, M., Rodriguez-Zapata, L.C., Hozak, P., and Castano, E. (2015). Fibrillarin from Archaea to human. Biol. Cell *107*, 159–174.

Ruggero, D., and Pandolfi, P.P. (2003). Does the ribosome translate cancer? Nat. Rev. Cancer *3*, 179–192.

Russell, J., and Zomerdijk, J.C.B.M. (2005). RNA-polymerase-I-directed rDNA transcription, life and works. Trends Biochem. Sci. *30*, 87–96.

Sen Gupta, A., and Sengupta, K. (2017). Lamin B2 modulates nucleolar morphology, dynamics, and function. Mol. Cell. Biol. *37*.

Tessarz, P., Santos-Rosa, H., Robson, S.C., Sylvestersen, K.B., Nelson, C.J., Nielsen, M.L., and Kouzarides, T. (2014). Glutamine methylation in histone H2A is an RNA-polymerase-I-dedicated modification. Nature *505*, 564–568.

Tollervey, D., Lehtonen, H., Carmo-Fonseca, M., and Hurt, E.C. (1991). The small nucleolar RNP protein NOP1 (fibrillarin) is required for pre-rRNA processing in yeast. EMBO J. *10*, 573–583.

(2017). Nuclear structure and dynamics. In Cell Biology, (Elsevier), pp. 143–160.